Activation pathways taking place at molecular copper precatalysts for the oxygen evolution reaction

Ham, C.J.M. van der; Isik, F.; Verhoeven, T.W.G.M.; Niemantsverdriet, J.W.; Hetterscheid, D.G.H.

Catalysis Today 290 (2017) 33–38

Contents lists available at ScienceDirect

Catalysis Today

journal homepage: www.elsevier.com/locate/cattod

Activation pathways taking place at molecular copper precatalysts for the oxygen evolution reaction

Cornelis J.M. van der Ham [a], Furkan Işık [a], Tiny W.G.M. Verhoeven [b], J.W. (Hans) Niemantsverdriet [c], Dennis G.H. Hetterscheid [a,*]

[a] Leiden Institute of Chemistry, Leiden University, 2300 RA Leiden, The Netherlands
[b] Department of Chemical Engineering and Chemistry, Eindhoven University of Technology, P.O. Box 513, 5600 MB Eindhoven, The Netherlands
[c] SynCat@DIFFER, Syngaschem BV, P.O. Box 6336, 5600 HH Eindhoven, The Netherlands

ARTICLE INFO

Article history:
Received 7 September 2016
Received in revised form
19 December 2016
Accepted 21 December 2016
Available online 7 January 2017

Keywords:
Water oxidation
Copper oxide
Catalyst activation

ABSTRACT

The activation processes of $[Cu^{II}(bdmpza)_2]$ in the water oxidation reaction were investigated using cyclic voltammetry and chronoamperometry. Two different paths wherein CuO is formed were distinguished. $[Cu^{II}(bdmpza)_2]$ can be oxidized at high potentials to form CuO, which was observed by a slight increase in catalytic current over time. When $[Cu^{II}(bdmpza)_2]$ is initially reduced at low potentials, a more active water oxidation catalyst is generated, yielding high catalytic currents from the moment a sufficient potential is applied. This work highlights the importance of catalyst pre-treatment and the choice of the experimental conditions in water oxidation catalysis using copper complexes.

1. Introduction

The water oxidation reaction is important to ensure future energy storage and sustainability. The reaction has been extensively studied in the presence of homogeneous water oxidation catalysts that predominantly are based on noble metals such as ruthenium [1–3] and iridium [4–9]. In particular in case of molecular ruthenium systems bearing bipyridine type ligands, mechanistic studies have provided the community with detailed insights how water oxidation catalysis occurs [10–12]. In case of other water oxidation catalysts the true active species turned out to be metal oxide deposits that were formed from their organometallic precursors under the harsh oxidative conditions applied [13–16]. In terms of atom abundance and economic viability, complexes that are based on first row transition metals are more interesting than their second and third row counterparts, albeit such systems typically don't operate well under acidic conditions. Due to substantial faster ligand dissociation kinetics at these first row transitions metals, control over the catalyst structure is considerably more cumbersome. Nevertheless, molecular catalysts in case of manganese [17], iron [18–20], cobalt [21] and since very recently copper [22–30] have been reported. Especially in case of the latter, ligand exchange kinetics are fast, and consequently several papers have appeared wherein copper oxides proved to be the competent catalytic species rather than their molecular precursors [31–35]. A fruitful strategy to prevent formation of copper oxides appears to lie with multi-denticity [29]. Nevertheless, also the copper bipyridine complexes, first reported by Mayer et al., appear to react exclusively *via* molecular sites [22,23], suggesting that discrimination between homogeneous *versus* heterogeneous catalysis is much more complex. From early cobalt polyoxometallate water oxidation chemistry the scientific community has already learned that the formation of which type of catalytic species is formed can be largely dependent on the exact reaction conditions applied, especially in case of highly dynamic systems [36–39].

Preliminary water oxidation studies in our lab in the presence of $[Cu^{II}(bdmpza)_2]$ ($bdmpza^-$ = bis(3,5-dimethyl-1H-pyrazol-1-yl)acetate, Fig. 1), a structure similar to the aforementioned copper bipyridine system, revealed that the observed water oxidation activity is strongly dependent on the electrochemical pretreatment of the molecular catalyst, even though the eventual catalytic experiments were carried out under the exact same conditions. In light of the discussion whether catalysis occurs at a homogeneous *versus* heterogeneous species and how one can control the activity of these catalytic species, the pretreatment dependence triggered us to investigate the catalyst activation pathways of $[Cu^{II}(bdmpza)_2]$ in detail. In this contribution we discuss two independent pathways to the formation of CuO, the true active

* Corresponding author.
E-mail address: d.g.h.hetterscheid@chem.leidenuniv.nl (D.G.H. Hetterscheid).

http://dx.doi.org/10.1016/j.cattod.2016.12.042
0920-5861/

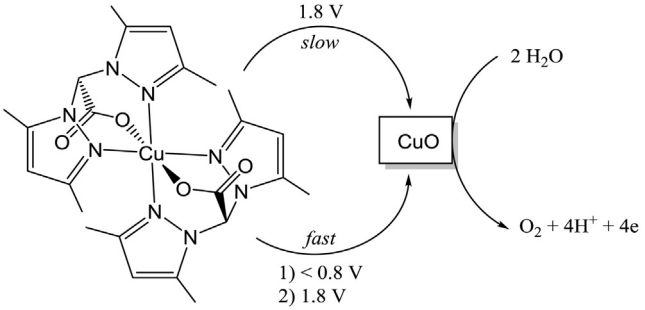

Fig. 1. Paths of activation observed for [Cu^{II}(bdmpza)$_2$].

species, wherein the observed reactivity is greatly activation path dependent.

2. Experimental

2.1. Complex synthesis

[Cu^{II}(bdmpza)$_2$] was obtained by dropwise addition of 0.33 mmol bdmpzaNa in 25 ml methanol to a solution of 0.33 mmol $Cu^{II}(OTf)_2$ in 25 ml methanol. After stirring for 30 min, part of the methanol was evaporated and diethyl ether was added to the reaction mixture to yield a blue-green precipitate overnight. The crystalline material was dried in vacuo and recrystallized from methanol at −20 °C, yielding [Cu^{II}(bdmpza)$_2$]. The infrared spectra of [Cu^{II}(bdmpza)$_2$] are in good agreement with previous reported data (see supporting info) [40]. ESI MS *m/z* (calc):558.2 (558.2, $[M]^+$ 580.2 (580.2, $[M+Na]^+$), 612.2 (612.2, $[M+Na+MeOH]^+$).

2.2. Electrochemical methods

All experiments were performed on an Autolab PGSTAT 128N. All electrochemical experiments were performed in one-compartment 25 ml glass cells in a three-electrode setup, using a gold working electrode (WE). In all cases a gold wire was used as a counter electrode and all experiments were measured against the reversible hydrogen electrode. The electrochemical cell was boiled twice in Millipore MilliQ water (>18.2 MΩ cm resistivity) prior to the experiment. The Au working electrode constisted of a disc and was used in a hanging meniscus configuration. The WE was cleaned by applying 10 V between the WE and a graphite counter electrode for 30 s in a 10% H_2SO_4 solution. This was followed by dipping the WE in a 6 M HCl solution for 20 s. The electrode was flame annealed, followed by electrochemical polishing in 0.1 M $HClO_4$, while scanning between 0 and 1.75 V *versus* RHE for 200 cycles at 1 V s^{-1}. Eventually 5 μl of a 18 mM solution of [Cu^{II}(bdmpza)$_2$] in ethanol was dropcasted onto the working electrode and dried in air. The electrolyte solutions were prepared from MilliQ water (>18.2 MΩ cm resistivity) and ≥99.9995% NaOH obtained from Sigma-Aldrich.

The electrochemical quartz crystal microbalance (EQCM) experiments were performed in a 3 ml Teflon cell purchased from Autolab. As a working electrode, an Autolab EQCM electrode was used, wherein a 200 nm gold layer (1.5 cm^2) was deposited on a quartz crystal. Since the hydrogen bubbles of the RHE reference electrode disturbed the frequency during the EQCM measurements, a Pd/H_2 reference electrode was prepared by applying a potential of −4.0 V between the Pd wire and a platinum counter electrode for approximately 10 min. Prior to the experiment the potential of the Pd/H_2 electrode relative to the RHE was determined. All EQCM data were corrected to the RHE scale. The sensitivity coefficient of the quartz crystal (c_f) was determined by deposition of $PbNO_3$. An electrolyte solution containing 10 mM $PbNO_3$ and 0.1 M $HClO_4$ was prepared. Cyclic voltammetry at 100 mV s^{-1} gave the relationship between the Δf and the amount of Pb deposited onto the electrode. The sensitivity coefficient was determined to be 1.26×10^{-8} g cm^{-2} Hz^{-1} (Fig. S3). For the catalytic experiments, 10 μl of an 18 mM solution of [Cu^{II}(bdmpza)$_2$] in ethanol was dropcasted onto the EQCM electrode, yet due to its geometry it was impossible to avoid that some [Cu^{II}(bdmpza)$_2$] was deposited on the quartz part of the assembly. The actual amount of catalytic material that is in contact with the working electrode is therefore overestimated.

During the online electrochemical mass spectrometry (OLEMS) measurements the gaseous products formed at the working electrode were collected *via* a hydrophobic tip (KEL-F with a porous Teflon plug) in close proximity to the surface of the working electrode and analyzed in a Pfeiffer QMS 200 mass spectrometer. An Ivium A06075 potentiostat was used in combination with the OLEMS experiments. A detailed description of the OLEMS setup is available elsewhere [40].

2.3. XPS

XPS measurements were carried out with a Thermo Scientific K-Alpha, equipped with a monochromatic small-spot X-ray source and a 180° double focusing hemispherical analyzer with a 128-channel detector. Spectra were obtained using an aluminium anode (Al Kα = 1486.6 eV) operating at 72 W and a spot size of 400 μm. Survey scans were measured at a constant pass energy of 200 eV and region scans at 50 eV. The background pressure was 2×10^{-8} mbar and during measurement 4×10^{-7} mbar Argon because of charge compensation.

Samples for XPS were prepared by chrono amperometry in 0.1 M NaOH at pH 13, using 0.8 cm^2 pyrolitic graphite discs as working electrodes. Prior to use, the electrodes were sanded with waterproof 2500 grit sandpaper. A total amount of 180 nmol [Cu^{II}(bdmpza)$_2$] was dropcasted onto the electrodes and the discs were used in a hanging meniscus configuration.

3. Results

The $bdmpza^-$ ligands of [Cu^{II}(bdmpza)$_2$] are centrosymmetrically arranged around the copper ion, forming a *trans*-CuN_4O_2 complex, wherein the copper site is coordinatively saturated [41]. However, it is not unprecedented that one of the ligand arms of $bdmpza^-$ dissociates in favor of coordination of water [42], providing an entry into catalysis at a molecular species. The redox chemistry of [Cu^{II}(bdmpza)$_2$] was explored by dropcasting the complex onto a gold working electrode (WE). Fig. 2 shows the cyclic voltammogram of 90 nmol [Cu^{II}(bdmpza)$_2$] dropcasted onto a 0.050 cm^2 (geometric surface area) gold electrode in a 0.1 M aqueous NaOH solution at pH 13. The experiment was started at 1.2 V *versus* RHE and scanned towards positive potentials initially. In the first scan relatively little catalytic current is observed, which contrasts the second and third scans. Scanning the potential up to 2.0 V *versus* RHE resulted in a small peak (designated 1 in Fig. 2) in the cyclic voltammogram, which does not exceed the current displaying that of a blank gold electrode under the same conditions (see Fig. S4). While starting above 1.2 V *versus* RHE and scanning into a positive direction first or scanning in negative direction immediately does not result in changes in the reduction chemistry. Below 1.2 V a series of sharp reduction peaks (2–5 in Fig. 2) can be observed that lie on top of a broad negative baseline current that starts roughly at 0.8 V *versus* RHE. The negative baseline current continues upon scanning into the positive direction until 0.8 V after which a very sharp oxidative peak (7) is observed at 0.9 V *versus* RHE.

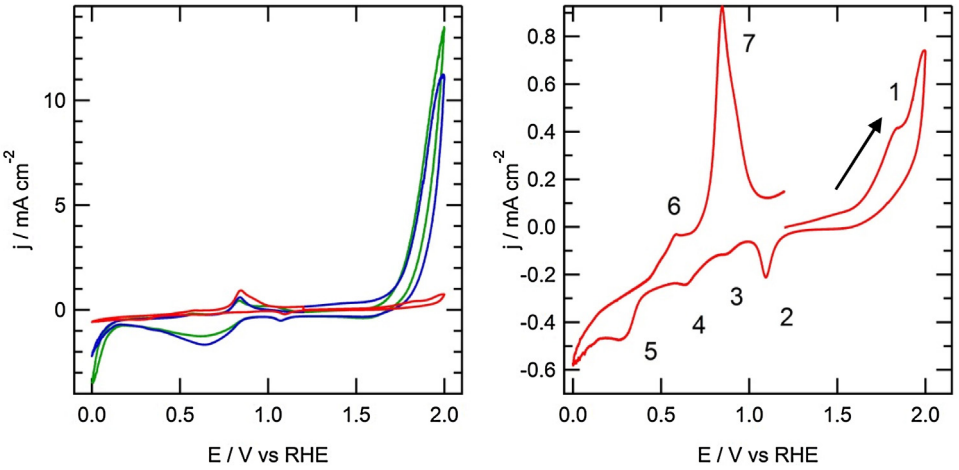

Fig. 2. The first three scans of a cyclic voltammetry experiment of [Cu^{II}(bdmpza)$_2$] in 0.1 M NaOH at a 100 mV s^{-1} scan rate (left). The first scan of the cyclic voltammetry (red) is depicted in magnified view separately (right) from the 2nd (blue) and 3rd scan (green). (For interpretation of the references to colour in this figure legend, the reader is referred to the web version of this article.)

With an onset of roughly 1.6 V *versus* RHE a substantial catalytic wave is observed in the cyclic voltammetry that greatly exceeds the oxidative current that was observed in the first scan. When an initial starting potential was selected below 0.8 V *versus* RHE, such a catalytic current can already be observed at the very first oxidative scan, suggesting it is triggered by an initial reduction of [Cu^{II}(bdmpza)$_2$]. In the second reductive scan a broad feature at 0.5 V *versus* RHE is observed followed by a catalytic reductive current with an onset at 0.2 V *versus* RHE. This latter catalytic feature is most likely due to reduction of dioxygen that is formed above 1.7 V *versus* RHE in the 2nd scan. From here on the redox features in the cyclic voltammogram do not further change upon potential cycling. The catalytic current does increase somewhat from scan 2–3, indicating that still more active water oxidation sites are formed on the WE.

The displayed catalytic activity in the presence of [Cu^{II}(bdmpza)$_2$] was further evaluated by chrono amperometry experiments using both gold (Fig. 3) and pyrolytic graphite electrodes. In this series of experiments 1.2 V *versus* RHE was selected as a standby potential as no oxidative or reductive currents were observed at this potential in the first scan of the voltammogram of [Cu^{II}(bdmpza)$_2$]. On gold an initial current of 7.2 μA cm^{-2} was observed after 120 s of amperometry at 2.0 V that steadily increases to 12 μA cm^{-2} after 30 min (Fig. 3). This suggests that some activation of [Cu^{II}(bdmpza)$_2$] to a (more) active catalytic species takes place under these oxidative conditions. In line with the oxidative current observed in the amperometry, online electrochemical mass spectrometry (OLEMS) data do show formation of some dioxygen over the course of time (Fig. 3, top panel).

X-ray photoelectron spectroscopy of [Cu^{II}(bdmpza)$_2$] that was kept at 2.0 V *versus* RHE for 10 min dropcasted on a pyrolytic graphite electrode shows two independent signals in the binding energy region of the 2p electrons of copper at 931.1 and 933.3 eV. The low binding energy peak (931.3 eV) can be due to either Cu metal or a Cu(I) species, such as Cu_2O The Cu LMM Auger peaks (not shown), falling in the binding energy range, exclude the presence of metallic Cu (which has a distinct peak at 565,5 eV), and, interestingly, also that of $Cu(OH)_2$. The signal at 933.3 eV is similar to that of CuO for which we find a binding energy of 933.4 eV (slightly higher values have been reported in literature: *i.e.* 933.9 eV [34], 933.7 eV [43], 933.8 eV [44]). The shake-up structure is mostly characteristic of CuO, except for the small but visible feature on the high binding energy side (about 942 eV), which is also present in the

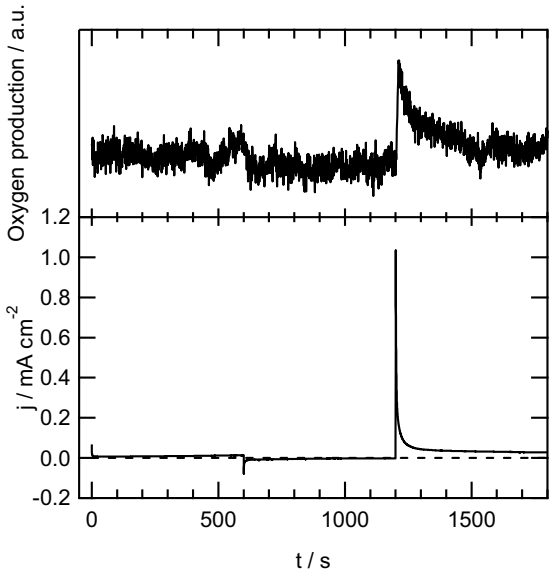

Fig. 3. Chrono amperometry of 360 nmol [Cu^{II}(bdmpza)$_2$] dropcasted onto a 0.72 cm^2 gold electrode (geometrical surface area) in 0.1 M NaOH. The potential was set at 2.0 V *versus* RHE for 600 s, then set to 0.0 V for another 600 s and then returned to 2.0 V for the last 600 s (bottom panel). The evolution of dioxygen was followed simultaneously using OLEMS (top panel).

spectrum of Cu_2O. Hence we interpret the *ex situ* XPS measurement of [Cu^{II}(bdmpza)$_2$] kept at 2.0 V *versus* RHE for 10 min to a mixture of Cu(I) and Cu(II) oxides, while the spectra show no evidence for Cu metal nor $Cu(OH)_2$.

Apparently [Cu^{II}(bdmpza)$_2$] slowly converts to CuO at 2.0 V *versus* RHE. Since CuO is a known water oxidation catalyst[45–47] and the catalytic activity increases upon prolonged electrolysis it seems likely that CuO is responsible for most – if not all –catalytic current. In fact at this point we have no reason to believe that any of the observed catalytic activity should be described to the [Cu^{II}(bdmpza)$_2$] species itself.

When the potential after the initial amperometry experiment at 2.0 V is set at 0.0 V for 10 min and then placed back at 2.0 V *versus* RHE, a considerably higher catalytic current is observed. This is in line with OLEMS data at this stage, which shows that a considerable amount of dioxygen is produced (Fig. 3, top panel). After 60 s a current of 56 μA cm^{-2} was recorded that slowly decreased

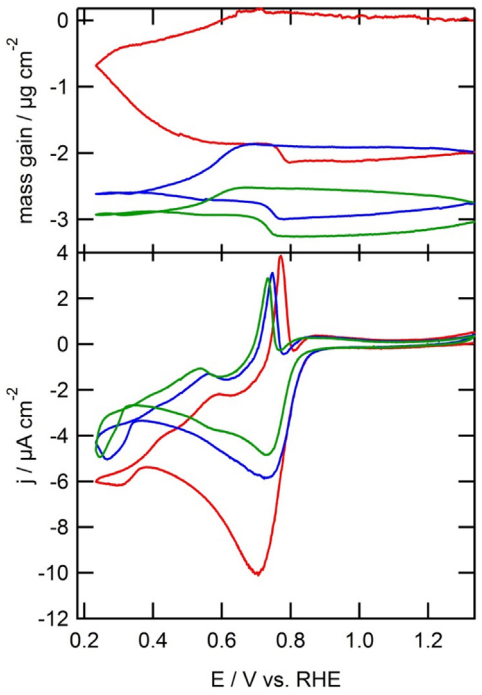

Fig. 4. Electrochemistry of [Cu^{II}(bdmpza)$_2$] combined with a quartz crystal microbalance showing the loss of mass of the electrode (top panel) during cyclic voltammetry (bottom panel) in a 0.1 M aqueous NaOH solution of pH 13. E_{start} = 1.3 V, scan rate = 1 mV s^{-1}.

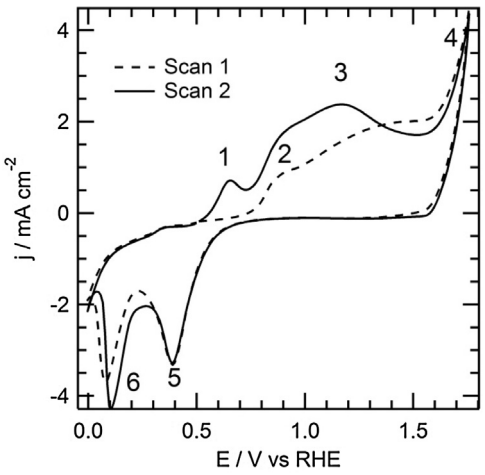

Fig. 5. Cyclic voltammogram of a polycrystalline Cu electrode at 100 mV s^{-1} in 0.1 M aqueous NaOH solution (pH 13). The experiment is started at 0.5 V *versus* RHE and scanned towards positive potentials first.

to 28 µA cm^{-2}. Even higher catalytic currents are obtained when [Cu^{II}(bdmpza)$_2$] is immediately reduced at 0 V and then brought to 2.0 V. X-ray photoelectron spectroscopy now only shows a single peak at 933.3 eV suggesting that full conversion to CuO has taken place. The decrease of the catalytic current upon prolonged electrolysis is most likely due to depletion of Cu^{2+} from the electrode under these conditions. It is likely that upon reduction [Cu^{II}(bdmpza)$_2$] converts to metallic copper(0) at the electrode interface that in turn is oxidized to CuO. For several related systems conversion of molecular species to copper(0) has been observed in relation to the catalytic hydrogen evolution reaction [48–50].

From the cyclic voltammetry in Fig. 2 it was observed that the reduction of [Cu^{II}(bdmpza)$_2$] on the electrode has a great influence on the current observed in the oxidative regime and is believed to proceed *via* initial formation of metallic copper. Electrochemical quartz crystal microbalance (EQCM) in combination with cyclic voltammetry is a powerful tool to gain insight into the processes taking place on the electrode. In these studies roughly 180 nmol [Cu^{II}(bdmpza)$_2$] in EtOH was dropcasted onto the EQCM electrode. Fig. 4 shows the EQCM of [Cu^{II}(bdmpza)$_2$] between 1.3 and 0.2 V *versus* RHE. The bottom panel shows the potential–current relationship from the CV, whereas the top panel shows the corresponding mass change of the quartz crystal, determined from the change in oscillation frequency of the quartz crystal simultaneously with the cyclic voltammetry experiment. At a scan rate of 1 mV s^{-1} a broad and clearly visible reduction peak is observed with an onset of 0.7 *versus* RHE, due to reduction of [Cu^{II}(bdmpza)$_2$] to copper(0). The features observed in the cyclic voltammetry upon reduction leading to formation of copper are strongly scan rate dependent. Similar to the cyclic voltammetry depicted in Fig. 2, a negative baseline is observed in both negative and positive scan. In addition to reduction of [Cu^{II}(bdmpza)$_2$] this in part may be due to reduction of some dioxygen that leaks into the Teflon EQCM cell. The top panel of Fig. 4 shows that the initial mass of the electrode does not change upon scanning the potential from 1.3 to 0.7 V *versus* RHE. Beyond the onset of the reduction wave at 0.7 V *versus* RHE in the cyclic voltammogram, the mass of the crystal starts to decrease, indicating that desorption of material from the electrode takes place. This mass decrease continues in the positive going scan and reaches a plateau at 0.4 V *versus* RHE.

The sharp oxidation peak observed at 0.8 V *versus* RHE is considerably less dependent on the scan rate. This is most likely a stripping peak [51], illustrated by a small and abrupt decrease in mass. The second and third scan show considerably less current and smaller mass changes than the first scan and is in agreement with a high conversion of [Cu^{II}(bdmpza)$_2$] to metallic copper at this stage. In Fig. 4, a total charge of 8.5 mC has passed through the WE to reduce [Cu^{II}(bdmpza)$_2$], which equals a total of 88 nmol electrons. A somewhat larger amount of 180 nmol [Cu^{II}(bdmpza)$_2$] was dropcasted onto the gold electrode, but it proved difficult to exclude large amounts of material from ending up on the quartz rather than on the gold surface which is electrochemically active. Moreover some of the charge flow may be due to reduction of dioxygen as it proved to be difficult to exclude air leaking into the Teflon EQCM cell. Nevertheless these numbers are in line with a considerable part of the dropcasted material to be reduced to copper in the EQCM experiment and agree with full conversion of [Cu^{II}(bdmpza)$_2$] to take place during prolonged amperometry at 0.0 V *versus* RHE.

The EQCM data in Fig. 4 shows that relatively little ligand (~20 nmol bdmpza equaling 5% of dropcasted bdmpza) is lost from the electrode interface during the reduction of [Cu^{II}(bdmpza)$_2$] to copper(0). Also the amount of copper lost to the solution at the copper stripping peak at 0.8 V *versus* RHE is limited (after three scans ~18 nmol Cu, 10% of all dropcasted copper).

In the cyclic voltammetry of polycrystalline copper a small oxidation wave is observed at 0.6 V *versus* RHE that is ascribed to oxidation of copper(0) to Cu_2O (Fig. 5, signal 1) [52]. A very similar oxidation wave is observed at 0.6 V in case of deposited [Cu^{II}(bdmpza)$_2$] (Figs. 2 and 4). Further oxidation to CuO, however, is considerably more facile in case of deposited [Cu^{II}(bdmpza)$_2$] compared to polycrystalline copper, which shows broad features (signals 2 and 3 in Fig. 5) as the result of oxidation of different crystal domains [51–53]. The copper deposit obtained from [Cu^{II}(bdmpza)$_2$] only shows a small and very sharp oxidation wave (Fig. 2, signal 7). We have been unable to reproduce these electrochemical features of using other sources of copper, including copper oxide nanoparticles, $Cu(OTf)_2$ and a polycrystalline copper electrode (see Fig. 5 and the supporting info). In all these cases copper is considerably easier removed from the electrode surface compared

to samples of $[Cu^{II}(bdmpza)_2]$. In line with the remarkable stability of the copper catalyst obtained from $[Cu^{II}(bdmpza)_2]$ compared to other sources of copper, also the observed catalytic current is more persistent and significantly higher. It appears that the bdmpza ligand has clear effect on the stability of the copper particles that are formed, and seems to prevent solvation of Cu^{2+} upon reoxidation of copper to the +II oxidation state. In line with such a hypothesis the presence of concentrated solutions of carbonate [54] and especially borate [34,55] have a dramatic influence on the stability and therefore activity of copper deposits under oxidative conditions. It seems that similar to coordinating anions, the bdmpza ligand has a stabilizing effect on copper oxide *versus* solvation, thereby posing an interesting application of the use of organic ligands and/or additives in heterogeneous water oxidation chemistry.

4. Conclusions

Two paths haven been identified wherein $[Cu^{II}(bdmpza)_2]$ is converted to CuO, which is the true active species in the water oxidation reaction. Under oxidative conditions $[Cu^{II}(bdmpza)_2]$ slowly converts to CuO and leads to moderate activity only. Initial reduction of $[Cu^{II}(bdmpza)_2]$ below 0.8 V *versus* RHE leads to initial formation of copper(0), which ultimately converts to CuO under catalytic conditions. This path leads to a substantial higher catalytic activity under the conditions explored. One therefore has to be very careful which standby and/or start potential is selected prior to catalytic water oxidation mediated by molecular copper complexes, as these settings may have a dramatic effect on the displayed catalytic activity as illustrated above. Also the $bdmpza^-$ ligand plays an important role in the observed catalytic activity, since drop-casting various other copper sources results in mediocre stability and activity. Clearly one cannot use such alternative copper sources convincingly as a control for the formation of active CuO nanoparticles. The precise mechanism wherein $bdmpza^-$ influences the catalytic activity is not well understood at present.

Acknowledgements

The authors gratefully acknowledge Dr. Tom van Dijkman and Prof. Dr. Elisabeth Bouwman for supplying the bdmpzaNa ligands used in this work. This work was financially supported by the ERC (StG 637556).

Appendix A. Supplementary data

Supplementary data associated with this article can be found, in the online version, at http://dx.doi.org/10.1016/j.cattod.2016.12.042.

References

[1] L.L. Duan, F. Bozoglian, S. Mandal, B. Stewart, T. Privalov, A. Llobet, L.C. Sun, A molecular ruthenium catalyst with water-oxidation activity comparable to that of photosystem II, Nat. Chem. 4 (2012) 418–423.
[2] R. Matheu, M.Z. Ertem, J. Benet-Buchholz, E. Coronado, V.S. Batista, X. Sala, A. Llobet, Intramolecular proton transfer boosts water oxidation catalyzed by a Ru complex, J. Am. Chem. Soc. 137 (2015) 10786–10795.
[3] J.J. Concepcion, J.W. Jurss, M.R. Norris, Z.F. Chen, J.L. Templeton, T.J. Meyer, Catalytic water oxidation by single-site ruthenium catalysts, Inorg. Chem. 49 (2010) 1277–1279.
[4] O. Diaz-Morales, T.J.P. Hersbach, D.G.H. Hetterscheid, J.N.H. Reek, M.T.M. Koper, Electrochemical and spectroelectrochemical characterization of an iridium-based molecular catalyst for water splitting: turnover frequencies, stability, and electrolyte effects, J. Am. Chem. Soc. 36 (2014) 10432–10439.
[5] R. Lalrempuia, N.D. McDaniel, H. Muller-Bunz, S. Bernhard, M. Albrecht, Water oxidation catalyzed by strong carbene-type donor-Ligand complexes of iridium, Angew. Chem. Int. Ed. 49 (2010) 9765–9768.
[6] A. Bucci, A. Savini, L. Rocchigiani, C. Zuccaccia, S. Rizzato, A. Albinati, A. Llobet, A. Macchioni, Organometallic iridium catalysts based on pyridinecarboxylate ligands for the oxidative splitting of water, Organometallics 31 (2012) 8071–8074.
[7] S.W. Sheehan, J.M. Thomsen, U. Hintermair, R.H. Crabtree, G.W. Brudvig, C.A. Schmuttenmaer, A molecular catalyst for water oxidation that binds to metal oxide surfaces, Nat. Commun. 6 (2015).
[8] J.D. Blakemore, N.D. Schley, D. Balcells, J.F. Hull, G.W. Olack, C.D. Incarvito, O. Eisenstein, G.W. Brudvig, R.H. Crabtree, Half-sandwich iridium complexes for homogeneous water-oxidation catalysis, J. Am. Chem. Soc. 132 (2010) 16017–16029.
[9] D.G.H. Hetterscheid, C.J.M. van der Ham, O. Diaz-Morales, M.W.G.M. Verhoeven, A. Longo, D. Banerjee, J.W. Niemantsverdriet, J.N.H. Reek, M.C. Feiters, Early stages of catalyst aging in the iridium mediated water oxidation reaction, Phys. Chem. Chem. Phys. 18 (2016) 10931–10940.
[10] J. Nyhlen, L.L. Duan, B. Akermark, L.C. Sun, T. Privalov, Evolution of O_2 in a seven-coordinate Ru^{IV} dimer complex with a $[HOHOH]^-$ bridge: a computational study, Angew. Chem. Int. Ed. 49 (2010) 1773–1777.
[11] J.J. Concepcion, M.K. Tsai, J.T. Muckerman, T.J. Meyer, Mechanism of water oxidation by single-site ruthenium complex catalysts, J. Am. Chem. Soc. 132 (2010) 1545–1557.
[12] Z.F. Chen, J.J. Concepcion, X.Q. Hu, W.T. Yang, P.G. Hoertz, T.J. Meyer, Concerted O atom-proton transfer in the O–O bond forming step in water oxidation, Proc. Natl. Acad. Sci. U. S. A. 107 (2010) 7225–7229.
[13] S. Fukuzumi, D.C. Hong, Homogeneous versus heterogeneous catalysts in water oxidation, Eur. J. Inorg. Chem. (2014) 645–659.
[14] B. Limburg, E. Bouwman, S. Bonnet, Molecular water oxidation catalysts based on transition metals and their decomposition pathways, Coordin. Chem. Rev. 256 (2012) 1451–1467.
[15] H. Junge, N. Marquet, A. Kammer, S. Denurra, M. Bauer, S. Wohlrab, F. Gartner, M.M. Pohl, A. Spannenberg, S. Gladiali, M. Beller, Water oxidation with molecularly defined iridium complexes: insights into homogeneous versus heterogeneous catalysis, Chem. Eur. J. 18 (2012) 12749–12758.
[16] J.D. Blakemore, N.D. Schley, G.W. Olack, C.D. Incarvito, G.W. Brudvig, R.H. Crabtree, Anodic deposition of a robust iridium-based water-oxidation catalyst from organometallic precursors, Chem. Sci. 2 (2011) 94–98.
[17] J. Limburg, J.S. Vrettos, L.M. Liable-Sands, A.L. Rheingold, R.H. Crabtree, G.W. Brudvig, A functional model for O–O bond formation by the O_2-evolving complex in photosystem II, Science 283 (1999) 1524–1527.
[18] J.L. Fillol, Z. Codola, I. Garcia-Bosch, L. Gomez, J.J. Pla, M. Costas, Efficient water oxidation catalysts based on readily available iron coordination complexes, Nat. Chem. 3 (2011) 807–813.
[19] K.G. Kottrup, D.G.H. Hetterscheid, Evaluation of iron-based electrocatalysts for water oxidation – an on-line mass spectrometry approach, Chem. Commun. 52 (2016) 2643–2646.
[20] W.C. Ellis, N.D. McDaniel, S. Bernhard, T.J. Collins, Fast water oxidation using iron, J. Am. Chem. Soc. 132 (2010) 10990–10991.
[21] D.J. Wasylenko, C. Ganesamoorthy, J. Borau-Garcia, C.P. Berlinguette, Electrochemical evidence for catalytic water oxidation mediated by a high-valent cobalt complex, Chem. Commun. 47 (2011) 4249–4251.
[22] S.M. Barnett, K.I. Goldberg, J.M. Mayer, A soluble copper-bipyridine water-oxidation electrocatalyst, Nat. Chem. 4 (2012) 498–502.
[23] D.L. Gerlach, S. Bhagan, A.A. Cruce, D.B. Burks, I. Nieto, H.T. Truong, S.P. Kelley, C.J. Herbst-Gervasoni, K.L. Jernigan, M.K. Bowman, S.L. Pan, M. Zeller, E.T. Papish, Studies of the pathways open to copper water oxidation catalysts containing proximal hydroxy groups during basic electrocatalysis, Inorg. Chem. 53 (2014) 12689–12698.
[24] J.S. Pap, L. Szyrwiel, D. Sranko, Z. Kerner, B. Setner, Z. Szewczuk, W. Malinka, Electrocatalytic water oxidation by Cu^{II} complexes with branched peptides, Chem. Commun. 51 (2015) 6322–6324.
[25] T. Zhang, C. Wang, S.B. Liu, J.L. Wang, W.B. Lin, A biomimetic copper water oxidation catalyst with low overpotential, J. Am. Chem. Soc. 136 (2014) 273–281.
[26] X.J. Su, M. Gao, L. Jiao, R.Z. Liao, P.E.M. Siegbahn, J.P. Cheng, M.T. Zhang, Electrocatalytic water oxidation by a dinuclear copper complex in a neutral aqueous solution, Angew. Chem. Int. Ed. 54 (2015) 4909–4914.
[27] M.T. Zhang, Z.F. Chen, P. Kang, T.J. Meyer, Electrocatalytic water oxidation with a copper(II) polypeptide complex, J. Am. Chem. Soc. 135 (2013) 2048–2051.
[28] Z.F. Chen, T.J. Meyer, Copper(II) catalysis of water oxidation, Angew. Chem. Int. Ed. 52 (2013) 700–703.
[29] P. Garrido-Barros, I. Funes-Ardoiz, S. Drouet, J. Benet-Buchholz, F. Maseras, A. Llobet, Redox non-innocent ligand controls water oxidation overpotential in a new family of mononuclear Cu-based efficient catalysts, J. Am. Chem. Soc. 137 (2015) 6758–6761.
[30] M.K. Coggins, M.T. Zhang, Z.F. Chen, N. Song, T.J. Meyer, Single-site copper(II) water oxidation electrocatalysis: rate enhancements with HPO_4^{2-} as a proton acceptor at pH 8, Angew. Chem. Int. Ed. 53 (2014) 12226–12230.
[31] T.T. Li, S. Cao, C. Yang, Y. Chen, X.J. Lv, W.F. Fu, Electrochemical water oxidation by in situ-generated copper oxide film from $[Cu(TEOA)(H_2O)_2][SO_4]$ complex, Inorg. Chem. 54 (2015) 3061–3067.
[32] X. Liu, H.X. Jia, Z.J. Sun, H.Y. Chen, P. Xu, P.W. Du, Nanostructured copper oxide electrodeposited from copper(II) complexes as an active catalyst for electrocatalytic oxygen evolution reaction, Electrochem. Commun. 46 (2014) 1–4.
[33] X. Liu, S.S. Cui, Z.J. Sun, P.W. Du, Copper oxide nanomaterials synthesized from simple copper salts as active catalysts for electrocatalytic water oxidation, Electrochim. Acta 160 (2015) 202–208.

[34] F.S. Yu, F. Li, B.B. Zhang, H. Li, L.C. Sun, Efficient electrocatalytic water oxidation by a copper oxide thin film in borate buffer, ACS Catal. 5 (2015) 627–630.
[35] X. Liu, S.S. Cui, M.M. Qian, Z.J. Sun, P.W. Du, In situ generated highly active copper oxide catalysts for the oxygen evolution reaction at low overpotential in alkaline solutions, Chem. Commun. 52 (2016) 5546–5549.
[36] S.J. Folkman, J.T. Kirner, R.G. Finke, Cobalt polyoxometalate $Co_4V_2W_{18}O_{68}^{10-}$: a critical investigation of its synthesis, purity, and observed V-51 quadrupolar NMR, Inorg. Chem. 5 (2016) 5343–5355.
[37] J.J. Stracke, R.G. Finke, Water oxidation catalysis beginning with 2.5 μM $[Co_4(H_2O)_2(PW_9O_{34})_2]^{10-}$: investigation of the true electrochemically driven catalyst at >=600 mV overpotential at a glassy carbon electrode, ACS Catal. 3 (2013) 1209–1219.
[38] J.J. Stracke, R.G. Finke, Electrocatalytic water oxidation beginning with the cobalt polyoxometalate $[Co_4(H_2O)_2(PW_9O_{34})_2]^{10-}$: identification of heterogeneous Co_{Ox} as the dominant catalyst, J. Am. Chem. Soc. 133 (2011) 14872–14875.
[39] J.W. Vickers, H.J. Lv, J.M. Sumliner, G.B. Zhu, Z. Luo, D.G. Musaev, Y.V. Geletii, C.L. Hill, Differentiating homogeneous and heterogeneous water oxidation catalysis: confirmation that $[Co_4(H_2O)_2$ $(\alpha\text{-}PW_9O_{34})_2]^{10-}$ Is a molecular water oxidation catalyst, J. Am. Chem. Soc. 135 (2013) 14110–14118.
[40] A.H. Wonders, T.H.M. Housmans, V. Rosca, M.T.M. Koper, On-line mass spectrometry system for measurements at single-crystal electrodes in hanging meniscus configuration, J. Appl. Electrochem. 36 (2006) 1215–1221.
[41] B. Kozlevcar, P. Gamez, R. de Gelder, W.L. Driessen, J. Reedijk, Unprecedented change of the Jahn-Teller axis in a centrosymmetric Cu^{II} complex induced by lattice water molecules – crystal and molecular structures of bis[bis(3, 5-dimethylpyrazol-1-yl)acetato]copper(II) and its dihydrate, Eur. J. Inorg. Chem. (2003) 47–50.
[42] B. Kozlevcar, A. Golobic, P. Gamez, I.A. Koval, W.L. Driessen, J. Reedijk, A tridentate bis(pyrazolyl) ligand binds to Cu(II), without using the pyrazole group: a very unusual coordination mode of the ligand Hbdmpb 1,3-bis(3,5-dimethylpyrazol-1-yl)-2-butanoic acid, Inorg. Chim. Acta 358 (2005) 1135–1140.
[43] M. Durando, R. Morrish, A.J. Muscat, Kinetics and mechanism for the reaction of hexafluoroacetylacetone with CuO in supercritical carbon dioxide, J. Am. Chem. Soc. 130 (2008) 16659–16668.
[44] J.F. Moulder, W.F. Stickle, P.E. Sobol, K.D. Bomben, Handbook of X-ray Photoelectron Spectroscopy, 1995, pp. 86–87.
[45] F. Yu, F. Li, B. Zhang, H. Li, L. Sun, Efficient electrocatalytic water oxidation by a copper oxide thin film in borate buffer, ACS Catal. 5 (2015) 627–630.
[46] X. Liu, S. Cui, Z. Sun, Y. Ren, X. Zhang, P. Du, Self-supported copper oxide electrocatalyst for water oxidation at low overpotential and confirmation of its robustness by Cu K-Edge X-ray absorption spectroscopy, J. Phys. Chem. C 120 (2016) 831–840.
[47] X. Liu, S. Cui, Z. Sun, P. Du, Copper oxide nanomaterials synthesized from simple copper salts as active catalysts for electrocatalytic water oxidation, Electrochim. Acta 160 (2015) 202–208.
[48] M. Kugler, J. Scholz, A. Kronz, I. Siewert, Copper complexes as catalyst precursors in the electrochemical hydrogen evolution reaction, Dalton Trans. 45 (2016) 6974–6982.
[49] X. Liu, H.F. Zheng, Z.J. Sun, A. Han, P.W. Du, Earth-abundant copper-based bifunctional electrocatalyst for both catalytic hydrogen production and water oxidation, ACS Catal. 5 (2015) 1530–1538.
[50] X. Liu, S.S. Cui, Z.J. Sun, P.W. Du, Robust and highly active copper-based electrocatalyst for hydrogen production at low overpotential in neutral water, Chem. Commun. 51 (2015) 12954–12957.
[51] J. Ambrose, R.G. Barradas, Dw Shoesmit, Rotating copper disk electrode studies of mechanism of dissolution-passivation step on copper in alkaline solutions, J. Electroanal. Chem. 47 (1973) 65–80.
[52] S.D. Giri, A. Sarkar, Electrochemical study of bulk and monolayer copper in alkaline solution, J. Electrochem. Soc. 163 (2016) I1252–I1259.
[53] J.M.M. Droog, C.A. Alderliesten, P.T. Alderliesten, G.A. Bootsma, Initial-stages of anodic-oxidation of polycrystalline copper electrodes in alkaline-solution, J. Electroanal. Chem. 111 (1980) 61–70.
[54] J.L. Du, Z.F. Chen, S.R. Ye, B.J. Wiley, T.J. Meyer, Copper as a robust and transparent electrocatalyst for water oxidation, Angew. Chem. Int. Ed. 54 (2015) 2073–2078.
[55] Y.Y. Shi, C. Gimbert-Surinach, T.T. Han, S. Berardi, M. Lanza, A. Llobet, CuO-functionalized silicon photoanodes for photoelectrochemical water splitting devices, ACS Appl. Mater. Interfaces 8 (2016) 696–702.